Hindawi
Advances in Materials Science and Engineering
Volume 2019, Article ID 6568057, 8 pages
https://doi.org/10.1155/2019/6568057

Research Article

Flexural Toughness of Basalt Fibre-Reinforced Shotcrete and Industrial-Scale Testing

Huazhe Jiao,[1] Yachuang Wu,[1] Xinming Chen,[1] and Yixuan Yang[2]

[1]*School of Civil Engineering, Henan Polytechnic University, Jiaozuo, Henan, China*
[2]*Institute of Recourses and Environment, Henan Polytechnic University, Jiaozuo, Henan, China*

Correspondence should be addressed to Yixuan Yang; yangyixuan@hpu.edu.cn

Received 19 June 2019; Accepted 1 October 2019; Published 31 October 2019

Academic Editor: María Criado

This study focuses on toughness enhancement of basalt fibre-reinforced shotcrete (BFRS). Four-point bending experiments of underground shooting and curing beams combined with a roadway-supporting deformation monitoring test were conducted. The flexural performance was analysed based on the toughness standards, namely, DBV-1998, JSCE SF-4, and nuclear magnetic resonance (NMR) pore testing. The results demonstrate that, given a basalt fibre (BF) dosage of 0–7.5 kg/m^3, 18 mm BF can significantly increase the residual stress under the same deformation, rather than the peak values of the flexural strength. Meanwhile, the trend in the flexural toughness increases to a peak at a dosage of 3–4.5 kg/m^3, followed by a declining curve. The pores from an NMR test can be divided into three types based on size: (1) closed pores, $R < 0.01\,\mu$m, (2) capillary pores, $0.01\,\mu\text{m} < R < 5\,\mu$m, and (3) connected pores, $R > 5\,\mu$m. The connected pores are detrimental, playing a crucial role in the shotcrete performance. Furthermore, the deformations of the roadway walls are significantly restrained by the BFRS, and the 80-day convergences are approximately 2 mm, which is only 25% of the control. Finally, the comprehensive results indicate that a dosage range of 3–4.5 kg/m^3 can demonstrate reasonable beneficial effects for the BFRS performance.

1. Introduction

Among the various types fibres, including steel [1], glass [2], polymeric [3], and carbon [4] fibres, basalt fibre (BF) is a new type of inorganic material extruded from melted basalt rock. The manufacturing of BF is similar to that of glass fibre, however, with less energy consumption and no additives, which makes it cheaper than glass or carbon fibres. Other advantages such as a high modulus, heat resistance, good resistance to a chemical attack [5], and an excellent interfacial shear strength [6] enable BF to be a good alternative as a reinforcing material in a concrete composite [7].

For BF in a concrete composite, a study on the chemical durability of BF was conducted by Ramachandran et al. as early as 1981, which demonstrated the potential of BF in reinforced concrete [8]. Studies have been conducted on a continuous basalt fibre-reinforced polymer (BFRP) as a strengthening material for concrete structures [9–12]. However, there have been limited studies on the effects of short cut BF on the properties of concrete. Sim et al. [13] demonstrated that basalt fibre reinforced concrete (BFRC) can improve the tensile strength and fracture elongation by 0.5- to 1- and 3- to 5-times, respectively, compared with ordinary concrete. Deb [14] tested the physical and mechanical properties of cement mortar reinforced by BF at 28 days and obtained the optimum dosage. Branston et al. [15] investigated the impact behaviour and damage evolution of BFRC and proposed that BF results in an obvious improvement of the impact toughness. Fu et al. [16] discussed the impact behaviour of BF-reinforced geopolymeric concrete under various high strain rates. The strength and deformation of the composites were further analysed, and a nonlinear viscoelastic constitutive model was proposed.

Fibres can effectively improve the mechanical properties of shotcrete and enhance the engineering properties, fatigue wear strength, postcracking toughness, and load-bearing capacity [17, 18]. Shotcrete is widely used in mining and underground spatial development [19, 20]. It is therefore

important to improve the shotcrete performance for the deep location and large deformation soft rock [21, 22]. Improvements in the flexural toughness have become a significant challenge, however.

Hence, to improve the BF utilisation, a mechanical behavioural analysis is the key aspect. Studies conducted at the experimental scale have made it challenging to conduct investigations at the industrial scale [23]. Cases supporting underground roadways are also rare.

In this study, to reveal the influence of BF on the mechanical properties and microstructure of shotcrete, specimens for a four-point-bending test were shot and cured underground to ensure the real processing and curing environment. The load-strain curve was analysed using both the DBV-1998 standard (German Concrete Society) from Germany [24] and the JSCE SF-4 standard from Japan [25]. The crucial roles of the BFRS microstructures were observed using a scanning electron microscope (SEM) and nuclear magnetic resonance (NMR).

More importantly, the underground roadway in a coal mine is supported by the recommended mixture ratio of the BFRS. The roadway convergence was monitored for 80 days to evaluate the BFRS performance.

2. Materials and Methods

2.1. Material Properties. Ordinary Portland cement was used as the binder, and the particle size of the coarse aggregate rock was less than 10 mm. The finer aggregate was crushed sand with a fineness modulus of 3.0, with a diameter of 0–3 mm. The BF used in this work is from Jintou Co., Shanxi Province, China; the parameters of which are listed in Table 1.

2.2. Specimen Preparation. Four-point-bending experiments of BFRS composite beams under a static load were conducted. To investigate the toughness enhancement mechanism, all beams were designed to fail under flexure rather than under a shear force. The details of the beam specimens are listed in Table 2, with a fibre dosage varying from 0 to 7.5 kg/m^3.

Furthermore, the beams were cut from shotcrete slabs cured underground, as shown in Figure 1. The dimensions of the slabs were 800 mm × 800 mm × 150 mm.

2.3. Four-Point-Bending Experiments. Based on the German standard DBV-1998, four-point-bending experiments were carried out on the beams using linear variable differential transformer (LVDT) sensors recording the beam deformation, as shown in Figure 1. The beam dimensions are 150 mm × 150 mm × 700 mm, the span is 600 mm, and the displacement control rate is 0.2 mm/min.

2.4. SEM Test. Liu used NMR and SEM to characterise the pore structure of CPB specimens [26]. JSM-6390LV from Japan Electronics, Co. was used in the SEM test, as shown in Figure 2.

2.5. NMR Test. The NMR specimen was 35 mm in diameter and 40 cylinders in height. To fill the pores with a liquid before the test, the specimen was treated using a vacuum negative pressure. The NMR equipment used is a Meso ME23-040V-I Microscopic Rocks Pore Structure Analysis and Imaging System, as shown in Figure 2. The intensity of the main magnetic field is 0.5 T.

3. Results and Discussion

3.1. Experiment Phenomena and Failure Mode

3.1.1. Load-Strain Curves. The results in Figure 3 indicate that the basalt fibre dosage has only a slight impact on the peak values of the flexural strength. The failure loads range from 11.3 to 13.5 kN, and the optimal dosage is 3 kg/m^3. The plain shotcrete beams displayed the characteristics of a complete brittle failure, with a maximum midspan deflection of 1.17 mm. Compared with the control specimen, the flexural strength at days 7 and 28 increased by 2.5%–9.8% and 1.6%–6.8%, respectively, at a fibre dosage of 1.5–7.5 kg/m^3.

More importantly, the BF can significantly increase the residual stress under the same deformation. As clearly shown in Figure 4, compared with the control, the specimens with a dosage of 3 or 7.5 kg/m^3 achieve a considerable residual stress. The specimen can obtain a residual stress of 10 kN at a deformation of 1.5-1.6 mm, 8 kN at 1.9–2.1 mm, and 4 kN at 3–3.5 mm. Meanwhile, the flexural strength at 1.5 and 4.5 kg/m^3 is also acceptable. By contrast, the control specimen gains an adverse performance.

3.1.2. Failure Mode. The failure mode of the BFRS beams becomes more complex with the dosage, as shown in Figure 5. Once the dosage is beyond 1.5 kg/m^3, the appearance of the cracks transforms from smooth to curved, where the cracked surfaces are rougher with a stepladder shape. Moreover, several subsidiary cracks appear along with the main crack. The beam specimen displays ductile failure features [27].

3.2. DBV-1998 Flexural Toughness Approach

3.2.1. DBV-1998 Method. The BFRS toughness and energy absorption capacity were evaluated using the concept of the equivalent flexural strength ($f_{eq,n}$) and deformation energy (D_n), rather than the residual strength (R) and flexural toughness index (I) in ASTM-C2018. This approach is shown in Figure 6 (fibre dosage of 7.5 kg/m^3) and equations (1)–(6). This method avoids the error caused by an artificial determination of the initial crack point.

The deformation energy D_n is as follows:

$$D_n = \int_0^{\delta} F(\delta)\mathrm{d}\delta, \tag{1}$$

$$D_n^f = D_n - D_n^c \ (n = 1, 2), \tag{2}$$

where D_n is the deformation energy, kN·mm; F is the load, kN; D_n^c is the energy absorption before beam cracking at

Table 1: Basalt fibre parameters.

Length (mm)	Single fibre diameter (in)	Density (g/cm^3)	Tensile strength (MPa)	Elastic modulus (GPa)	Fracture elongation
18	13	2.65	4,100–4,800	80–100	2.7%–3.4%

Table 2: Concrete proportioning.

Cement (kg/m^3)	Coarse aggregate <10 mm (kg/m^3)	Fine aggregate (kg/m^3)	Accelerator (kg/m^3)	Water (kg/m^3)
440	880	880	17.6	260

(a) (b) (c)

Figure 1: Beam specimen preparation: (a) underground concrete shot and curing, (b) slab cutting, and (c) beam specimen with a crack detector.

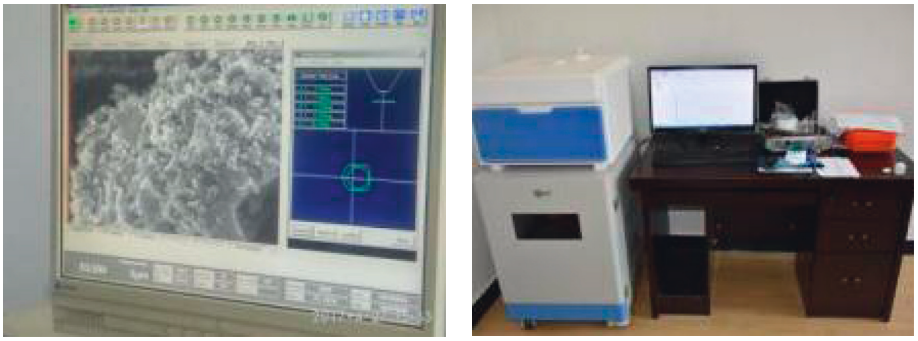

(a) (b)

Figure 2: (a) SEM and (b) NMR test.

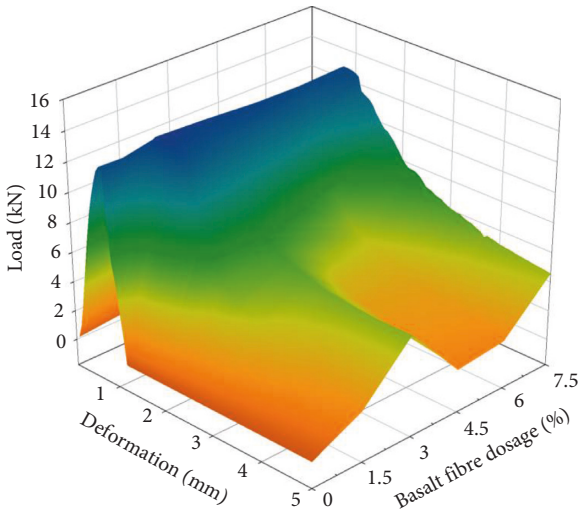

Figure 3: Load-strain curves of different specimens.

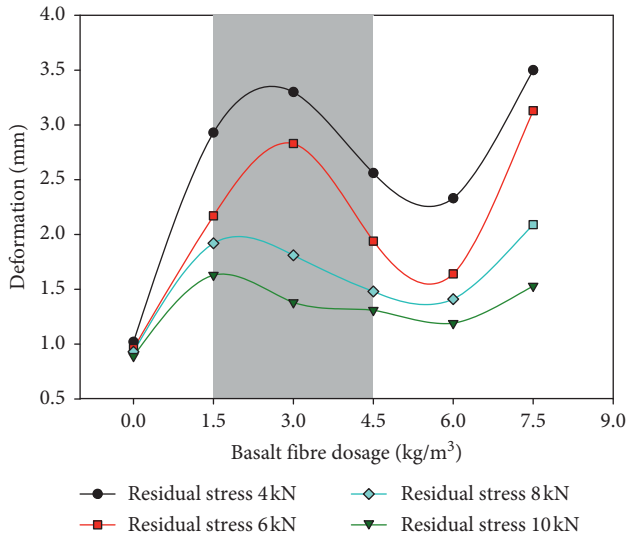

Figure 4: Residual flexural strength after failure.

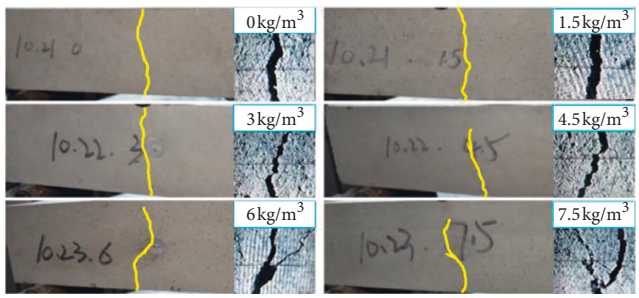

Figure 5: Failure and crack mode.

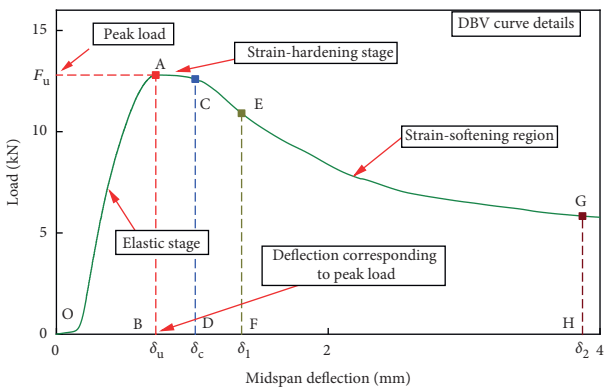

Figure 6: Calculation of DBV-1998 standard flexural toughness.

deformation δ ($\delta_0 + 0.3$ mm); δ is the midspan deflection, mm; D_n^f is the energy absorption at location n in a load-strain curve, kN·mm; and δ_0 is the midspan deflection at the peak load F_u, mm.

The equivalent flexural strength $f_{eq,n}$ is as follows:

$$F_{eq,1} = \frac{D_1^f}{0.5}, \tag{3}$$

$$f_{eq,1} = \frac{F_{eq,1} \times L}{bh^2}, \tag{4}$$

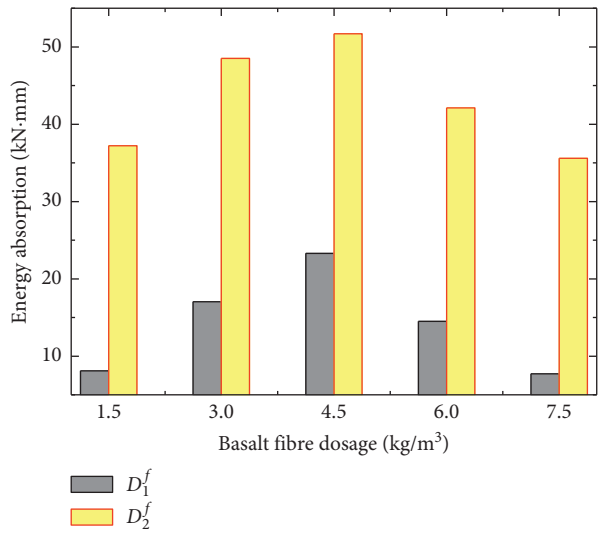

Figure 7: Deformation energy of DBV-1998.

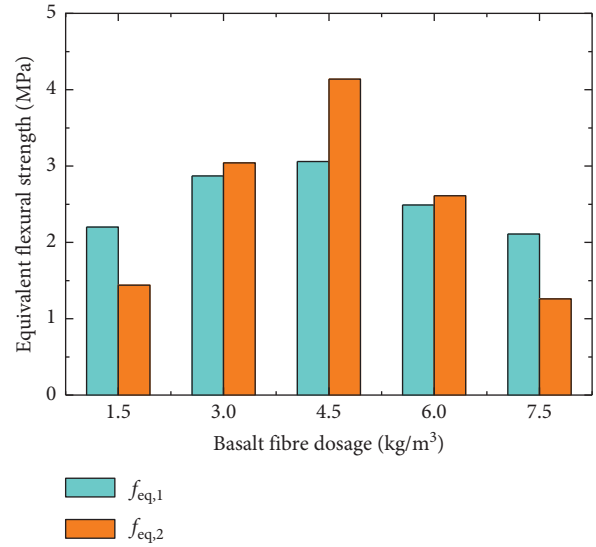

Figure 8: Equivalent flexural strength of DBV-1998.

$$F_{eq,2} = \frac{D_2^f}{3}, \tag{5}$$

$$f_{eq,2} = \frac{F_{eq,2} \times L}{bh^2}, \tag{6}$$

where $F_{eq,1}$ and $F_{eq,2}$ are the equivalent flexural strengths at midspans δ_1 and δ_2, N; f is the flexural strength at δ_1 and δ_2, MPa; D_1^f is the deformation energy at δ_1 ($\delta_1 = \delta_0 + 0.65$ mm), kN·mm; D_2^f is the deformation energy at δ_2 ($\delta_2 = \delta_0 + 3.15$ mm), kN·mm; and L, b, and h are the dimensions (length, width, and height, respectively) of the beams, mm.

3.2.2. DBV-1998 Results. The beam toughness is significantly improved by the BF, as shown in Figure 7.

Firstly, in terms of the deformation energy, the energy increases with the dosage but decreases after a dosage of beyond 4.5 kg/m^3. The optimal deformation energy is 29.5 and 57.9 N·m at deformations δ_1 and δ_2, respectively. The performance enhancement by BF is 4.5, 6, 3, 1.5, and 7.5 kg/m^3, as shown in Figure 8.

In the same way, the equivalent flexural strength shows a similar tendency. At a dosage of 4.5 kg/m^3, the equivalent flexural strength ($F_{eq,1}$, $F_{eq,2}$) obtained is 4.14 MPa and is 3.06 MPa under a standard deformation, which are 2.87- and 1.39-times that of the 1.5 kg/m^3 specimen, respectively. However, the flexural performance decreases once the dosage is beyond 4.5.

3.3. JSCE SF-4 Flexural Toughness Approach

3.3.1. JSCE SF-4 Method. To conduct further evaluation of the toughness, the JSCE SF-4 standard was applied to the beam result analysis.

The JSCE approach takes the equivalent flexural strength f_e as the main index to evaluate the flexural toughness of the BFRS. It is notable that, differing from DBV-1998, the JSCE approach only considers the flexural toughness index when the deflection is $L/150$, obeying the following equation:

$$f_e = \frac{\Omega_k L}{bh^2 \delta_k}, \tag{7}$$

where f_e is the equivalent flexural strength, MPa; Ω_k is the area under the load-strain curve at a midspan deflection of $L/150$, Nm; and δ_k is the deflection at a midspan deflection of $L/150$, mm.

The ratio of equivalent bending strength to the initial crack strength f_{cr} is defined as the bending toughness ratio.

$$f_{cr} = \frac{F_{cr} L}{bh^2}, \qquad R_e = \frac{f_e}{f_{cr}}, \tag{8}$$

where f_{cr} is first flexural crack strength, MPa; and F_{cr} is first flexural crack load, N.

3.3.2. JSCE SF-4 Results. The JSCE SF-4 results shown in Figure 9 further support the previous observational studies. The equivalent flexural strength (f_e) is slightly less than the first flexural crack strength (f_{cr}) at a deflection of $L/150$. The f_e peak at 4.5 kg/m^3 is 3.51 MPa. The effective weight of the dosage has the same rank as in the DBV-1998 approach.

In summary, the comprehensive results show a clear trend in the flexural toughness, increasing to a peak followed by a declining curve with the BF dosage. The dosage range of 3–4.5 kg/m^3 demonstrates reasonable beneficial effects regarding the BFRS performance.

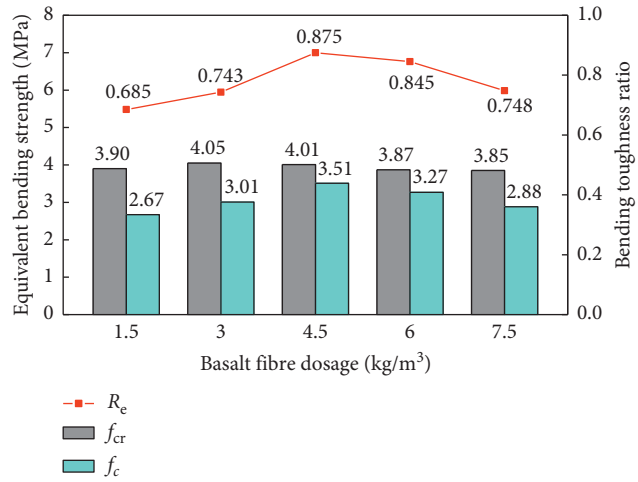

Figure 9: Equivalent bending strength of JSCE SF-4.

4. Microstructure

4.1. SEM Results. The enhanced functionality of BF in shotcrete is drawn from two main sources, namely, the interface bonding and the cracking control.

Firstly, the interface bonding between the fibre and shotcrete is as shown in Figure 10. The basalt fibre surface is covered by a compact cement hydration substrate. The AFt and C-S-H gel tightly wrap the BF, which can form a larger mechanical interlocking. In addition, the cement and BF are the same type of silicate materials, which have a good chemical compatibility [28].

4.2. NMR Results. As a heterogeneous composite cementitious material, internal defects will significantly affect the mechanical properties. Nuclear magnetic resonance (NMR) technology plays an important role in pore size distribution studies [29].

The total porosity ranges from 1.92% to 3.02% and increases with the fibre dosage, as shown in Figure 11.

To further confirm the microstructure, the pores can be divided into three types according to the size (pore diameter, R) distribution:

(i) Closed pore, $R < 0.01\ \mu$m

(ii) Capillary pore, $0.01\ \mu\text{m} < R < 5\ \mu$m

(iii) Connected pore, $R > 5\ \mu$m

The detailed results are shown in Figures 12 and 13.

In particular, for the three types of content in the shotcrete blocks, closed pores account for 63.3%–72.4%; capillary pores, 22.7%–29.9%; and connected pores, 0.3%–14%. Thus, connected pores are more sensitive to the dosage than the other two types.

The specimen at a fibre dosage of 3 kg/m^3, in line with most of the closed and bottom connected pores [30], obtains the optimal flexural strength peak, as shown in Figure 3. It is interesting to note that, for a dosage of 4.5 kg/m^3, the amount of cementitious pores is higher than that in plain concrete, whereas the amount of connected pores is lower

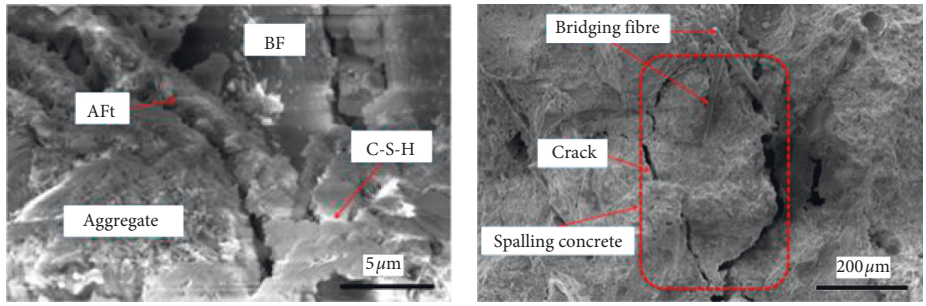

(a) (b)

Figure 10: Bonding between BF and C-S-H matrix: (a) interface bonding and (b) crack control.

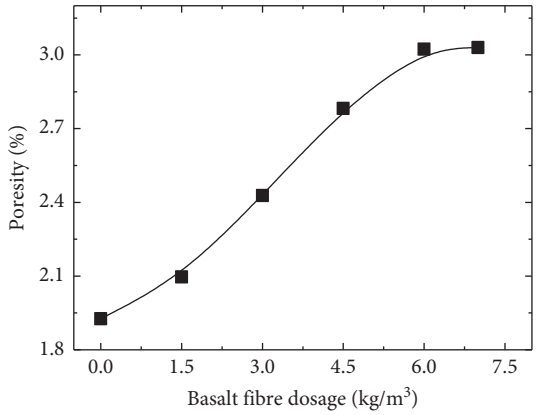

Figure 11: Porosity versus basalt fibre dosage.

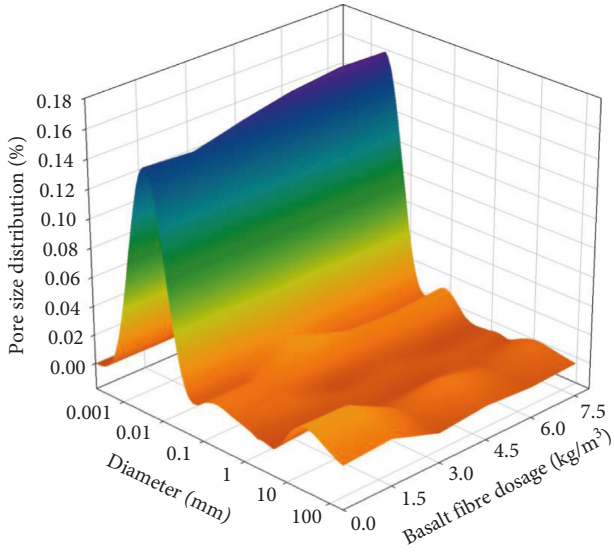

Figure 12: Pore size distribution at different fibre dosages.

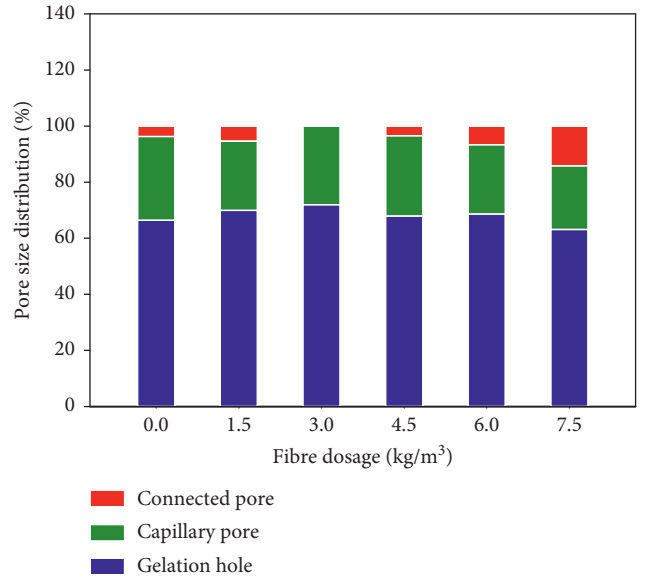

Figure 13: Pore size distribution of three types of pores.

than that of plain concrete; in addition, the specimen toughness also achieves considerable results. More importantly, at a dosage of 7.5 kg/m^3, the connected pores account for 14.03%, corresponding to a lower flexural strength.

Taking the above observations into account, it is important to note that the closed pores are beneficial in terms of strength. In contrast, the connected pores are detrimental, which plays a crucial role in shotcrete performance.

5. Industrial-Scale Test

5.1. Underground Roadway Shotcrete Support. An *in-situ* shot test was conducted along the roadways of the Zhaogu Coal Mine, China, at five different locations using dosages of 1.5–7.5 kg/m^3 and compared with the control location. The convergent deformation of the sidewall was monitored at each dosage after the final setting, as shown in Figure 14.

5.2. Convergence Monitoring Results. It is important to note that the deformation of the roadway walls was significantly restrained by the BFRC as compared with the control specimen, as shown in Figure 15. During the 80-day monitoring period, the control specimen roadway deformed by 8 mm. Meanwhile, the convergence of the 1.5 and 7.5 kg/m^3 basalt fibre shotcrete roadways was 4 mm, which is approximately 50% that of the control. Furthermore, at dosages of 3, 4.5, and 6 kg/m^3, the roadway convergences were almost 2 mm, which is only 25% that of the control.

The period during which the roadway deformation tends to be stable is significantly shortened in contrast with the control. The deformation of the fibre shotcrete supporting

Figure 14: Shotcrete support of underground roadway: (a) concrete *in-situ* shot, (b) wall convergence monitoring, and (c) BF distribution on shotcrete surface.

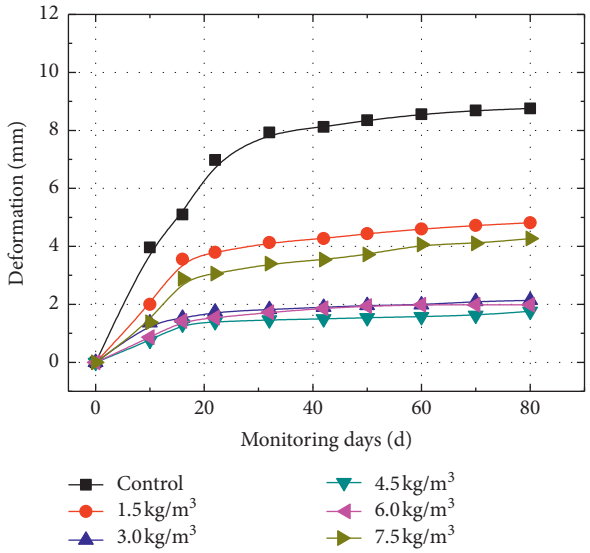

Figure 15: Convergent deformation curve of the roadway.

roadway tends to become stable within 16 to 18 days, reaching close to 70% of the final deformation. However, the control requires 30 days. Moreover, the 15-day deformation supported by shotcrete at 3, 4.5, and 6 kg/m^3 is 1.32–1.52 mm, reaching 75% of the 80-day deformation, which is a considerable effect.

The control of the roadway deformation is due to the uniform distribution of fibres and the toughness of the BFRS. Firstly, as shown in Figure 14(c), the in-site shotcrete is dense, and a random distribution of BF can be observed at the concrete layer surface [31].

By contrast, the BFRS achieved a higher flexural strength under the same deformation, and the BF can restrain the concrete layer cracks through a slip debonding effect. Subsequently, the BFRS can effectively restrain the surrounding rock deformation. Taking the above results of the analysis into account, the optimum ratio is recommended to be 3–4.5 kg/m^3.

6. Conclusion

(1) The basalt fibre dosage has only a slight impact on the peak values of the flexural strength. Compared with the control specimen, the flexural strength at day 7 and 28 increased 2.5%–9.8% and 1.6%–6.8%, respectively, at a fibre dosage of 1.5–7.5 kg/m^3.

(2) The BF can significantly increase the residual stress under the same deformation. There is a clear trend in the flexural toughness, increasing to a peak followed by a declining curve with the BF dosage. The dosage range of 3–4.5 kg/m^3 demonstrates acceptable beneficial effects regarding the BFRS performance.

(3) The total porosity ranges from 1.92% to 3.02%, increasing with the BF dosage. The pores can be divided into three types according to the size distribution, namely, closed pores (<0.01 μm), capillary pores, and connected pores (>5 μm). Closed pores are beneficial in terms of strength, whereas connected pores are detrimental and are sensitive to the dosage, which plays a crucial role in the shotcrete performance.

(4) The deformation of the roadway walls is significantly restrained by the BFRS, and at dosages of 3, 4.5, and 6 kg/m^3, the convergences of the roadways are almost 2 mm over an 80 day period, which is only 25% that of the control. The period of stability in the roadway deformation is thus greatly shortened in contrast with the control.

Data Availability

The data used to support the findings of this study are available from the corresponding author upon request.

Conflicts of Interest

The authors declare that there are no conflicts of interest regarding the publication of this paper.

Acknowledgments

This work was funded by the National Natural Science Foundation of China Projects (51701094, 51834001, and 51574013), the Key Technology and Technology Projects for the Prevention and Control of Major Accidents in Safety Production, China (Henan-0005-2016AQ), the Key Research Project Plan of Colleges and Universities in Henan

Province (16A440003), and the Open Funding of Henan Province Colleges and Universities Deep Mine Construction Key Discipline Open Laboratory (2015KF-01).

References

[1] S. P. Singh and S. K. Kaushik, "Fatigue strength of steel fibre reinforced concrete in flexure," *Cement and Concrete Composites*, vol. 25, no. 7, pp. 779–786, 2003.

[2] T. Deák and T. Czigány, "Chemical composition and mechanical properties of basalt and glass fibers: a comparison," *Textile Research Journal*, vol. 79, no. 7, pp. 645–651, 2009.

[3] Q. Ma, Z. Yang, Y. Gu, M. Li, S. Wang, and Z. Zhang, "Permeabilities along fiber direction of ramie bundles and through-thickness of ramie fabric stack for liquid composite molding," *Journal of Reinforced Plastics and Composites*, vol. 36, no. 1, pp. 40–52, 2017.

[4] J. Sun, X. Yao, X. Tian, C. Jingliang, and W. Yi, "Damage characteristics of CFRP laminates subjected to multiple lightning current strike," *Applied Composite Materials*, vol. 26, no. 3, pp. 745–762, 2019.

[5] V. Lopresto, C. Leone, and I. De Iorio, "Mechanical characterisation of basalt fibre reinforced plastic," *Composites Part B: Engineering*, vol. 42, no. 4, pp. 717–723, 2011.

[6] P. Davies and W. Verbouwe, "Evaluation of basalt fibre composites for marine applications," *Applied Composite Materials*, vol. 25, no. 2, pp. 299–308, 2018.

[7] C. H. Jiang, T. J. McCarthy, D. Chen, and Q. Q. Dong, "Influence of basalt fiber on performance of cement mortar," *Key Engineering Materials*, vol. 426-427, pp. 93–96, 2010.

[8] B. E. Ramachandran, V. Velpari, and N. Balasubramanian, "Chemical durability studies on basalt fibres," *Journal of Materials Science*, vol. 16, no. 12, pp. 3393–3397, 1981.

[9] C. Yuan, W. Chen, T. M. Pham, and H. Hao, "Bond behavior between basalt fibres reinforced polymer sheets and steel fibres reinforced concrete," *Engineering Structures*, vol. 176, pp. 812–824, 2018.

[10] L. Ding, X. Liu, X. Wang, H. Huang, and Z. Wu, "Mechanical properties of pultruded basalt fiber-reinforced polymer tube under axial tension and compression," *Construction and Building Materials*, vol. 176, pp. 629–637, 2018.

[11] J. Shi, X. Wang, Z. Wu, and Z. Zhu, "Fatigue behavior of basalt fiber-reinforced polymer tendons under a marine environment," *Construction and Building Materials*, vol. 137, pp. 46–54, 2017.

[12] F. Elgabbas, P. Vincent, E. A. Ahmed, and B. Brahim, "Experimental testing of basalt-fiber-reinforced polymer bars in concrete beams," *Composites Part B: Engineering*, vol. 91, pp. 205–218, 2016.

[13] J. Sim, C. Park, and D. Y. Moon, "Characteristics of basalt fiber as a strengthening material for concrete structures," *Composites Part B: Engineering*, vol. 36, no. 6-7, pp. 504–512, 2005.

[14] S. Deb, "The impact of basaltic fibre on selected physical and mechanical properties of cement mortar," *Composite Materials*, vol. 7, pp. 286–290, 2012.

[15] J. Branston, S. Das, S. Y. Kenno, and C. Taylor, "Mechanical behaviour of basalt fibre reinforced concrete," *Construction and Building Materials*, vol. 124, pp. 878–886, 2016.

[16] Q. Fu, D. Niu, J. Zhang et al., "Dynamic compressive mechanical behaviour and modelling of basalt–polypropylene fibre-reinforced concrete," *Archives of Civil and Mechanical Engineering*, vol. 18, no. 3, pp. 914–927, 2018.

[17] M. Khooshechin and J. Tanzadeh, "Experimental and mechanical performance of shotcrete made with nanomaterials and fiber reinforcement," *Construction and Building Materials*, vol. 165, pp. 199–205, 2018.

[18] E. S. Bernard, "Age-dependent changes in post-crack performance of fibre reinforced shotcrete linings," *Tunnelling and Underground Space Technology*, vol. 49, pp. 241–248, 2015.

[19] J. F. Dong, Q. Y. Wang, and Z. W. Guan, "Material properties of basalt fibre reinforced concrete made with recycled earthquake waste," *Construction and Building Materials*, vol. 130, pp. 241–251, 2017.

[20] J. H. Liu, R. D. Wu, and Y. C. Zhou, "Experiment of bursting liability of deep underground concrete under complex stress conditions," *China Coal Society*, vol. 43, pp. 79–86, 2018.

[21] H. Lu, C. Qi, Q. Chen, D. Gan, Z. Xue, and Y. Hu, "A new procedure for recycling waste tailings as cemented paste backfill to underground stopes and open pits," *Journal of Cleaner Production*, vol. 188, pp. 601–612, 2018.

[22] V. Marinos, "Tunnel behaviour and support associated with the weak rock masses of flyash," *Journal of Rock Mechanics and Geotechnical Engineering*, vol. 6, no. 3, pp. 227–239, 2014.

[23] Y. Ghernouti and B. Rabehi, "FRP-confined short concrete columns under compressive loading: experimental and modeling investigation," *Journal of Reinforced Plastics and Composites*, vol. 30, no. 3, pp. 241–255, 2011.

[24] P. Zhang, Y.-N. Zhao, Q.-F. Li, P. Wang, and T.-H. Zhang, "Flexural toughness of steel fiber reinforced high performance concrete containing nano-SiO_2 and fly ash," *The Scientific World Journal*, vol. 2014, Article ID 403743, 11 pages, 2014.

[25] J. J. Li, C. J. Wan, J. G. Niu, L. F. Wu, and Y. C. Wu, "Investigation on flexural toughness evaluation method of steel fiber reinforced lightweight aggregate concrete," *Construction and Building Materials*, vol. 131, pp. 449–458, 2017.

[26] L. Liu, Z. Fang, C. Qi, B. Zhang, L. Guo, and K.-I. Song, "Experimental investigation on the relationship between pore characteristics and unconfined compressive strength of cemented paste backfill," *Construction and Building Materials*, vol. 179, pp. 254–264, 2018.

[27] S. Cao, W. Song, and E. Yilmaz, "Influence of structural factors on uniaxial compressive strength of cemented tailings backfill," *Construction and Building Materials*, vol. 174, pp. 190–201, 2018.

[28] Y. Wang, M. Fall, and A. Wu, "Initial temperature-dependence of strength development and self-desiccation in cemented paste backfill that contains sodium silicate," *Cement and Concrete Composites*, vol. 67, pp. 101–110, 2016.

[29] Q. Chen, Q. Zhang, A. Fourie, and C. Xin, "Utilization of phosphogypsum and phosphate tailings for cemented paste backfill," *Journal of Environmental Management*, vol. 201, pp. 19–27, 2017.

[30] W. Sun, K. Hou, Z. Yang, and Y. Wen, "X-ray CT three-dimensional reconstruction and discrete element analysis of the cement paste backfill pore structure under uniaxial compression," *Construction and Building Materials*, vol. 138, pp. 69–78, 2017.

[31] D. Wu, Y. Hou, T. Deng, Y. Chen, and X. Zhao, "Thermal, hydraulic and mechanical performances of cemented coal gangue-fly ash backfill," *International Journal of Mineral Processing*, vol. 162, pp. 12–18, 2017.